Front. Phys. 11(4), 113301 (2016)
DOI 10.1007/s11467-016-0565-6

REVIEW ARTICLE

Laser cooling of internal degrees of freedom of molecules

R. Horchani

College of Arts and Applied Sciences, Dhofar University, Salalah, Oman

E-mail: horchani@phy.au.dk, ridha.horchani@yahoo.fr

Received November 29, 2015; accepted January 14, 2016

Optical pumping techniques using laser fields combined with photo-association of ultracold atoms leads to control of the vibrational and/or rotational population of molecules. In this study, we review the basic concepts and main steps that should be followed, including the excitation schemes and detection techniques used to achieve ro-vibrational cooling of Cs_2 molecules. We also discuss the extension of this technique to other molecules. In addition, we present a theoretical model used to support the experiment. These simulations can be widely used for the preparation of various experiments because they allow the optimization of several important experimental parameters.

Keywords cold molecule, photo-association, optical pumping, vibrational and rotational cooling

PACS numbers 33.20.Vq, 33.20.Wr

Contents

1 Introduction

A variety of fields require robust and selective methods of performing population transfer in quantum systems. We can cite fundamental tests in physics, molecular clocks, molecular spectroscopy, ultracold reactions, controlled photochemistry, and quantum computation. In particular, the precise control of both the internal and external degrees of freedom of cold and ultracold molecules becomes very attractive and promises new insight and advances in various domains of physics [1–3] and modern physical chemistry [4–6]. Several theoretical approaches have been proposed to control the internal degrees of freedom of cold molecules, such as the use of an external cavity to favor spontaneous emission toward the lowest ro-vibrational level [7] or the controlled interplay of coherent laser fields and spontaneous emission via quantum interference between different transitions [8–11]. From the experimental point of view, molecules are more difficult to control than atoms because of their complex internal structure. However, cold molecule formation has been achieved using different approaches that can be roughly grouped into two main classes: direct cooling of preformed molecules and indirect cold molecule formation by assembling cold or ultracold atoms [1]. In summary, two major challenges have been faced, the first is the decrease in the translational temperature of molecules (analogous to atom cooling) and the second is the reduction of the internal ro-vibronic energy. Ultimately, experimental efforts have focused on the control of the external degrees of freedom, leading to impressive achievements: one-dimensional transverse laser cooling [12] and longitudinal slowing [13] of a SrF beam, (more recently) one- and two-dimensional laser cooling with magneto-optical trapping of polar YO molecules [14], and Sisyphus cool-

© Higher Education Press and Springer-Verlag Berlin Heidelberg 2016

ing of electrically trapped polyatomic CH_3F molecules [15]. Other techniques have also been developed to coherently transfer molecular populations from one hyperfine level to another (Cs_2 [16], KRb [17]).

2 Production of molecules

Photo-association (PA) of atoms in atomic vapors is a well known process [18–21] in which two atoms collide in the presence of a photon of suitable energy $h\nu_L$ to create molecules in a ro-vibrational level (v,J) of an excited electronic state Ω. In the case of cesium molecules studied here, the PA can be described according to the following reaction:

$$\mathrm{Cs}(6s,\mathrm{F}) + \mathrm{Cs}(6s,\mathrm{F}) + h\nu_L \rightarrow \mathrm{Cs}_2^*(\Omega(6s+6p_j); v, J).$$

In this case, two atoms in a hyperfine level F of the $6s$ ground state absorb a photon of energy $h\nu_L$ and red-detuned from the atomic transition energy ($6s + 6p_j$, $j = \frac{1}{2}$ or $\frac{3}{2}$) in such a way they create a molecule in a ro-vibrational level (v,J) of an excited electronic state Ω related to one of the asymptotic ($6s + 6p_j$, $j = \frac{1}{2}$) or ($6s + 6p_j$, $j = \frac{3}{2}$).

Depending on the shape of the excited state potential, the excited molecules have a short lifetime of a few tens of nanoseconds; most often, they decay by spontaneous emission into two free "hot" atoms with a large relative kinetic energy, or into ro-vibrational levels of the lowest stable electronic states, which is the case of interest for the production of translationally cold molecules.

2.1 Molecules in the singlet state

The PA process used to produce cold cesium molecules in the singlet ground electronic state ($X^1\Sigma_g^+$, hereafter referred to as X) is achieved in a cesium magneto-optical trap in which nearly 10^8 atoms are trapped at a temperature of $T \approx 100$ μK using a clockwise (CW) Titanium:Sapphire laser with an intensity of up to 300 W/cm^2, it is pumped by an Ar^+ laser and has a spectral bandwidth smaller than 1 MHz; it can be tuned in a range between 700 nm to 1100 nm. The scheme is schematically presented in Fig. 1(a). The PA laser excites a pair of atoms to the ro-vibrational level (v, $J = 8$) at 11730.1245 cm^{-1} which is roughly 2 cm^{-1} below the $6s + 6p_{3/2}$ asymptote of the lowest $1_g(6s + 6p_{3/2})$ long-range molecular potential. At short distances, this potential is coupled to the lowest $1_g(6s + 5d_{5/2})$ potential through several avoided crossings induced by the spin-orbit interaction. The $v = 0$ level of this potential is predicted to be very close to the $(6s + 6p_{3/2})$ dissociation energy. By spontaneous emission via a two-photon cascade, the excited molecules end to the X ground electronic state via the $0_u^+(6s + 6p_{1/2})$ potentials, producing nearly 10^6 molecules per second. Here, we note that one-photon spontaneous emission favors the decay to ro-vibrational levels of the triplet electronic state $a^3\Sigma_u^+$, as reported in the first observation of the formation of translationally cold molecules [22]. However, this state, at the average internuclear distance of 8.73 a_0, corresponds to the range of the repulsive wall so that only "hot" atoms could be formed.

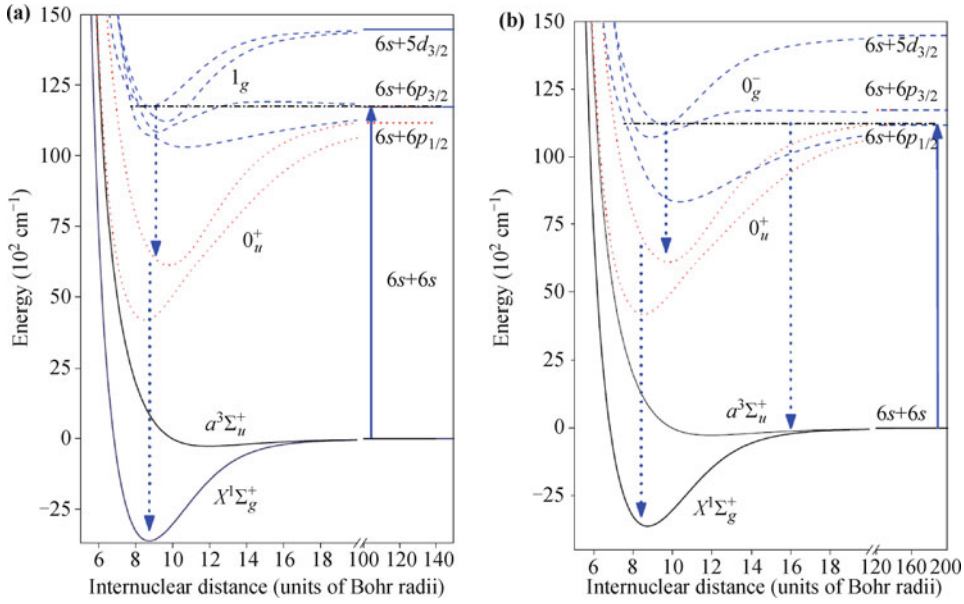

Fig. 1 Formation of cesium molecules in the ground electronic state by Photo-association through $1_g(6s + 6p_{3/2})$ **(a)** and $0_u^+(6s + 6p_{1/2})$ **(b)** states. The solid line arrows correspond to the laser excitation, the dotted line arrows represent spontaneous emission paths.

Recently, we identified another efficient mechanism of formation of cesium molecules in the X ground state [23]. The transitions involved in this mechanism are shown in Fig. 1(b). Here, the PA laser is used to excite long-range vibrational levels of the 0_g^- $(6s + 6p_{1/2})$ state. In the first 20 cm^{-1} below the atomic asymptote, vibrational levels are coupled to certain inner potential curves that presumably belong to the upper 0_g^- $(6s + 6p_{3/2})$ and 0_g^- $(6s+6p_{5/2})$ states. Because the 0_g^- state has gerade symmetry, any one-photon spontaneous decay ends up either as dissociating pairs or as the $\Omega = 0_u^{-/+}$, 1_u and 2_u components of the $A^1\Sigma_u^+$ or $b^3\Pi_u$ state located at intermediate energies. The 2_u state should be metastable, nevertheless, a resonant coupling with the $0_u^+(A^1\Sigma_u^+)$ state allows for a decay of the $0_u^+(A^3\Pi_u)$ component into the X ground state.

2.2 Molecules in the triplet state

To produce cesium molecules in the triplet electronic state $a^3\Sigma_u^+$ (hereafter referred to as the a state) we use an efficient PA scheme called giant line, G1 [22]. The frequency of the PA laser is set at 11730.0422 cm^{-1}, which corresponds to the vibrational level $v = 103$ of the 0_g^- $(6s + 6p_{3/2})$ state.

The potential 0_g^- $(6s + 6p_{3/2})$, described in Refs. [24, 25], has a potential curve with a distinct double-well shape, with a deep inner well with an equilibrium distance of roughly 10 a.u. and a shallow outer well caused by the competition between the long-range electrostatic interaction between the $6s$ and the $6p$ atoms (varying as R^{-3}, where R is the internuclear distance) and the spin-orbit interaction, which couples the $(1)^3\Sigma_g^+(6s+6p)$ state and the $(1)^3\Pi_g(6s + 6p)$ state. To our knowledge, spectroscopy of the inner well, which matches the $(1)^3\Pi_g$ state, is not yet available. In contrast, the outer well is well represented by an analytical asymptotic model [26], which accurately accounts for all available spectroscopic data given in Ref. [25]. Because of the potential barrier between the two wells, the outer well presents a favorable Condon point at intermediate internuclear distances (roughly 15 a.u.) that favors spontaneous emission towards vibrational levels of the triplet state (see Fig. 2).

Note that the photo-association process works mostly to form molecules in the triplet state [27]. However, by combining the PA process with the technique of conversion described in [28], we are able to produce large samples of ultracold molecules in the ground electronic state. In the case of cesium, this process forms twice the number of molecules in the ground electronic state than any other PA scheme.

Table 1 summarizes the frequencies of photoassociation that can be experimentally used to produce molecules either in the singlet state or in the triplet state.

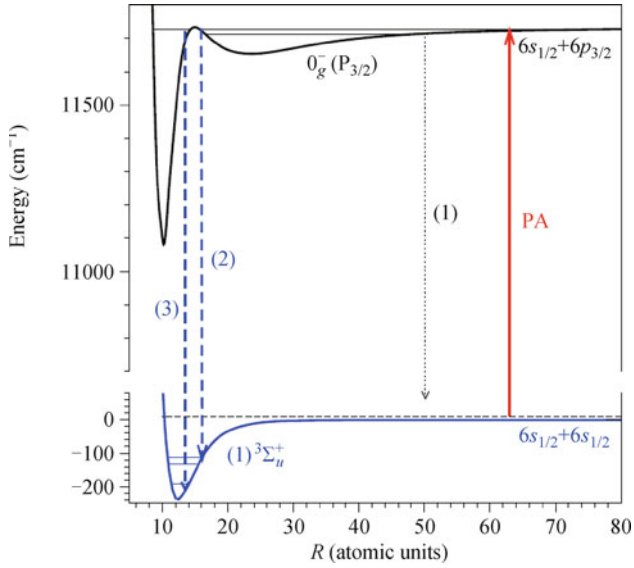

Fig. 2 Photo-association scheme (arrow labeled with PA) used to produce deeply-bound ultracold Cs_2 molecules in the $a^3\Sigma_u^+(6s+6s)$ state [arrows (2) and (3)]. Arrow (1) shows the decay of excited molecules by spontaneous emission into two "hot" atoms.

Table 1 Experimental values of PA frequencies used to produce cesium molecules.

State	PA	Frequency (cm^{-1})
$X^1\Sigma_g^+$	1_g $(v, J = 8)$	11730.1245
	$0_g^-(P_{1/2})$ $(v = 26, J = 2)$	11167.15855
$a^3\Sigma_u^+$	$0_g^-(P_{3/2})$ $(v = 103)$	11730.0422
	$0_g^-(P_{3/2})$ $(v = 79)$	11725.61
	$0_g^-(P_{3/2})$ $(v = 80)$	11725.7422

2.3 Detection

The scheme of detection is shown in Fig. 3. The formed Cs_2 molecules are ionized by resonance-enhanced two-photon ionization (RE2PI) through the excited $C^1\Pi_u(6s + 5d)$ or $D^1\Sigma_u^+(6s + 5d)$ molecular intermediate state for molecules formed in the X state and through the $(3)^3\Sigma_g^+$ molecular intermediate state for molecules formed in the a state. RE2PI detection uses a pulsed dye laser (DCM) spectral bandwidth of 0.5 cm^{-1}) pumped by the second harmonic of a pulsed Nd:YAG laser (repetition rate: 10 Hz, duration: 7 ns) to ionize the molecules. The formed ions are then quickly extracted from the MOT region and are accelerated toward a pair of micro-channel plates (MCPs) by applying a static electric field. The ions are detected through a time-of-flight mass spectrometer. By scanning the RE2PI wavelength in the available range (15800 – 16100 cm^{-1}), we obtain an ionization spectrum in which the peaks that appear correspond to vibrational transitions from either the triplet

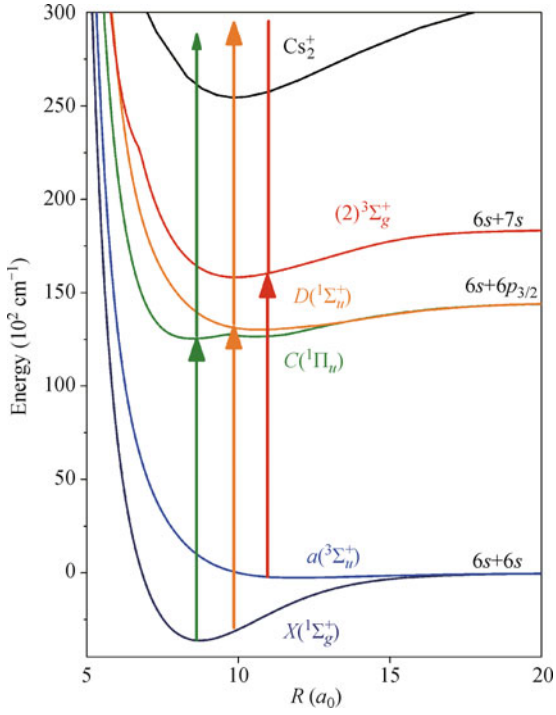

Fig. 3 Scheme used to detect vibrational populations (*solid up arrows*) by RE2PI. In the case of the X state, the probed spectral range has two distinct possible transitions through either $C^1\Pi_u$ or $D^1\Sigma_u^+$, however in the case of a state, molecules are detected through $(3)^3\Sigma_g^+$ state.

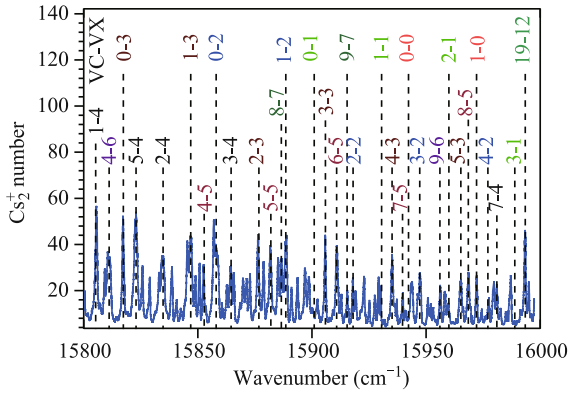

Fig. 4 RE2PI spectrum of Cs_2 molecules obtained after a PA process through the 0_g^- $(6s+6p_{1/2})$ state. Transition labels $v_C \leftarrow v_X$ are extracted from computed Franck–Condon factors between vibrational levels of the spectroscopically known C and X states.

state or the X state. An example of RE2PI is shown in Fig. 4. The observed ionization lines are assigned based on the spectroscopy given in Refs. [29–31]. Any change of the population of any vibrational level in the X or a state introduced by an additional laser light can be seen via a clear change in the relative intensities of the lines present in the spectrum. The molecular distribution among different vibrational levels can thereby be monitored. However, this method, because of its low resolution, remains unable to analyze the rotational distribution of the molecular sample.

3 Vibrational cooling by optical pumping

3.1 Basic principle

The principle of optical pumping has been successfully used to decrease the vibrational temperature of NaCs [32] and cool molecular ions [33, 34]. The ro-vibrational cooling scheme has been experimentally realized. In this study, for simplicity, we do not consider any hyperfine structure. However, hyperfine structural splitting is typically in the MHz range, which can be resolved and manipulated by generating side bands in the laser spectrum [34].

The operating principle of vibrational cooling, as performed in Refs. [35] and [36], is based on the so-called "luminorefrigeration" process proposed by Kastler [37] in 1950 to accumulate sodium atoms in the lowest state of the hyperfine manifold. Later, luminorefrigeration was also used to lower the "J" value of Cs_2 molecules [38].

The proposed method relies on the accumulation of the molecular population in a particular state via spontaneous emission. Accumulation can be achieved by isolating a closed ro-vibronic transition using a suitable laser spectrum and forcing the target state to be a "dark" state of the system, and thus, to not interact with the light and participate in the repeated absorption-spontaneous emission cycles. The simultaneous excitation of several vibrational levels is achieved using a broadband laser tuned to the transitions between the different vibrational levels labeled v_X and v_B, belonging, respectively, to the X ground electronic state and to an excited electronic state. In the cesium case we used $B^1\Pi_u$ (hereafter referred as B state) as an excited state. Starting from a given vibrational distribution of molecules in the X state, the absorption-spontaneous emission cycles lead, through optical pumping, to a redistribution of the population into the ground state according to the following scheme:

$$\mathrm{Cs}(v_X) + h\nu_{laser} \rightarrow \mathrm{Cs}(v_B) \rightarrow \mathrm{Cs}(v'_X) + h\nu_{em}, \qquad (1)$$

where $h\nu_{laser}$ and $h\nu_{em}$ correspond to the energies of the laser and of the spontaneously emitted photons, respectively.

Thanks to the broadband character of the laser, which permits repetition of the pumping process from multiple vibrational v_X levels. We remove all of the frequencies corresponding to the excitation of a selected vibrational level from the laser spectrum, and thereby, make it im-

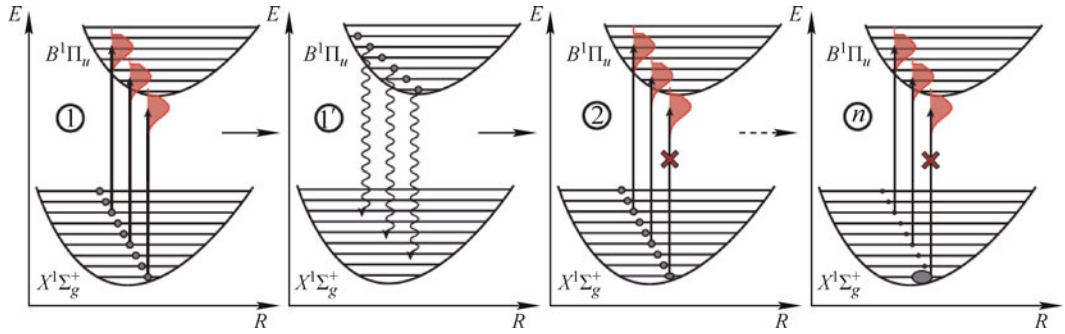

Fig. 5 Vibrational cooling of cesium molecules: (1) All molecular population is simultaneously excited by using shaped femtosecond pulses. (2) Redistribution of molecular population among the various vibrational levels by spontaneous emission. (3) Suppression of all frequencies that excite the ground vibrational state which makes it a "dark" state of the system. (i) After a sufficient number of steps all molecular population is accumulated to the ground vibrational level.

possible for an interaction with the laser to occur (the selected level is now a dark state). As time progresses, a series of absorption-spontaneous emission cycles described by Eq. (1) leads to an accumulation of the molecules in the selected level v_X (see Fig. 5).

The experimental demonstration of vibrational cooling consists of a comparison of RE2PI spectra of molecules before and after turning the femtosecond laser on. As shown in Fig. 6, the application of the shaped laser significantly modifies the photo-ionization spectrum. Intense resonance peaks appear; they correspond to the transition $v_X = 0 \rightarrow v_X = 0$–3, which are mostly absent in the original PA spectrum. This result reveals a net increase in the population at $v_X = 0$. The intensity of the lines indicates a very efficient transfer of the molecules in the lowest vibrational level, meaning a vibrational cooling of cesium molecules. Taking into account the efficiency of the detection ($\prec$10%), the detected ion signal corresponds to approximately 1,000 molecules at the $v_X = 0$ level, corresponding to a flux of $v_X = 0$ molecules of several 10^5 per second. The vibrational pumping toward $v = 0$ is very efficient only at low vibrational levels ($v_X \leqslant 10$).

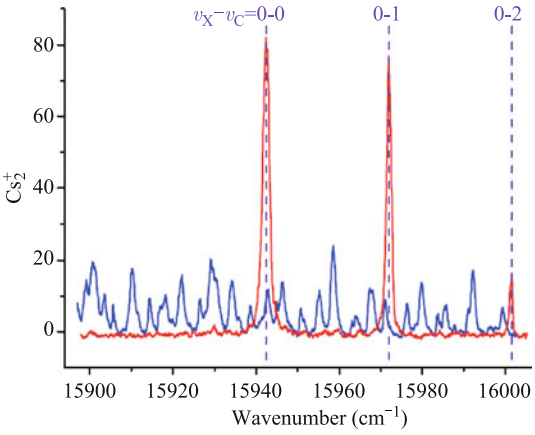

Fig. 6 Photo-ionisation spectra, the presence of the shaped femtosecond radiation results to the observation of strong lines corresponding to transitions from the ground vibrational level (*red line*) which were absent in the spectrum acquired without its presence (*blue line*).

3.2 Theoretical modeling

We have modeled the optical pumping in a simple way based on the information from the potential energy curves (PECs) for the particular molecular system. It is not necessary to initially know the precise distribution of the molecular population, because the large number of excitation-relaxation circles redistributes the molecular population in such a way that the final distribution does not depend on the initial distribution, as long as all of the initially populated states lie within the range of the broadband laser. However, in the simulation, we start from a molecular distribution close to the experimental distribution, which is obtained from a fit of the detection spectrum.

Figure 7 shows the optical pumping process, as it is used in our simulations. The process is divided in two steps: the femtosecond pulse excitation (absorption) from ground electronic state (X state) to the excited electronic state (B state) and the spontaneous emission from the B state to the X state.

The small pulse duration ($\leqslant$100 fs) leads us to neglect spontaneous emission during the absorption step, as its contribution to the final molecular population distribution is very small. Stimulated emission is also neglected because of the small femtosecond laser intensity. Using the known potential curves of the chosen molecular system and their rotational constants [30, 39], we calculate the ro-vibrational energy levels and the Franck–Condon (FC) factors for the transitions. The average laser intensity is very low, which corresponds to a perturbative regime, and thus, we assume that the excitation probability is simply proportional to the laser spectral den-

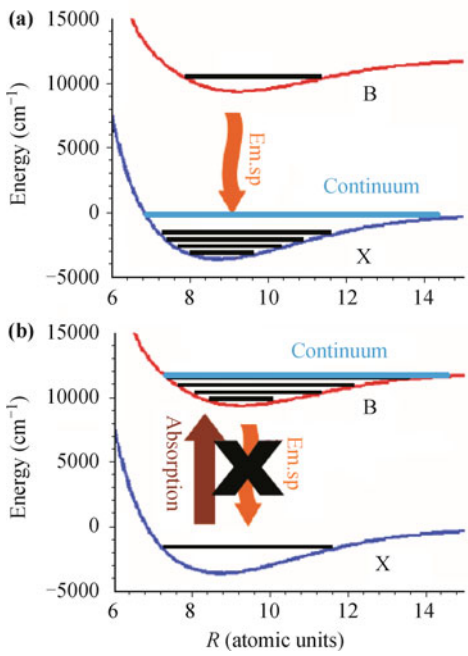

Fig. 7 The two physical process with which the rate equations used in the simulations of the vibrational cooling are associated. **(a)** The spontaneous emission step, in which molecules relax from a vibrational levels of the excited electronic state B to vibrational levels of the ground electronic state X. **(b)** The absorption step, in which vibrational levels of the X state are excited towards several vibrational levels of the B state. in this step, both excitation and spontaneous emission occur; however, in our simulations this spontaneous emission is omitted (see text for details).

sity at the transition frequencies, the FC factor, and the Hönl–London factor. During the excited state lifetime (15 ns), less than one photon is absorbed and, as a consequence, we assumed total population decay before another pulse is sent, i.e., 12.5 ns later. Other processes, such as three-photon direct ionization by the broadband laser or predissociation, are taken into account in the simulation.

In the perturbative approach, the distribution of molecules in the various vibrational levels is described in absorption by

$$P_{v_X}^{(n+1)} = P_{v_X}^{(n)} - \sum_{v_B} A_{v_B v_X} P_{v_X}^{(n)},$$

$$P_{v_B}^{(n+1)} = \sum_{v_X} A_{v_B v_X} P_{v_X}^{(n)},$$

and in emission by

$$P_{v_X}^{(n+2)} = P_{v_X}^{(n+1)} + \sum_{v_B} E_{v_X v_B} P_{v_B}^{(n+1)}.$$

$P_{v_X}^{(n)}$ and $P_{v_B}^{(n)}$ denote the population of the vibrational levels v_X and v_B of the ground and the excited electronic states, respectively, at the stage number n of the process. $A_{v_X v_B}$ denotes the ratio at which molecular populations are transferred from one vibrational level v_X to any v_B accessible by the laser bandwidth. Similarly, $E_{v_B v_X}$ denotes molecular population decay by spontaneous emission from one vibrational level v_B to v_X. These rates are proportional to

$$A_{v_X v_B} \propto FC_{v_X v_B} (D_{v_X v_B})^2 I_{laser, v_X v_B},$$
$$E_{v_X v_B} \propto FC_{v_X v_B} (D_{v_X v_B})^2 \omega_{v_X v_B}^3.$$

$FC_{v_X v_B}$, $(D_{v_X v_B})^2$ and $\omega_{v_X v_B}$ correspond to the FC factor, the dipole moment, and the transition frequency of the vibrational transition, respectively. In the harmonic approximation of the potential curves, the FC factors are given by the following formula:

$$|\langle v_X = 0 | v_B = 0 \rangle|^2 = \frac{\sqrt{\omega_X \omega_B}}{\omega_X + \omega_B} e^{-\frac{\mu (r_{eB} - r_{eX})^2 \omega_X \omega_B}{\hbar(\omega_X + \omega_B)}},$$

where μ is the reduced mass, ω_X and ω_B are the vibrational angular frequencies, and r_{eX} and r_{eX} are the equilibrium positions. As a consequence, after N absorption emission cycles,

$$P^{(2N)} = M^N P^{(0)},$$

with $M_{ij} = (1 + EA)_{ij} - \sum_k A_{ki}\delta_{ij} = \delta_{ij} + \sum_k (E_{ik} A_{kj} - A_{ki}\delta_{ij})$.

The simulations prove to be valuable, because, they can be used for the estimation of parameters that cannot be experimentally determined, the most important being the overall efficiency of the vibrational cooling technique. For example, in Ref. [23], we showed that vibrational pumping toward $v_X = 0$ is very efficient only for low vibrational levels ($v_X \leqslant 10$). This result is confirmed by our simulation, as shown in Fig. 8, where the pumping efficiency from a given v_X toward $v_X = 0$ is a given function of the vibrational levels, which is due only to the

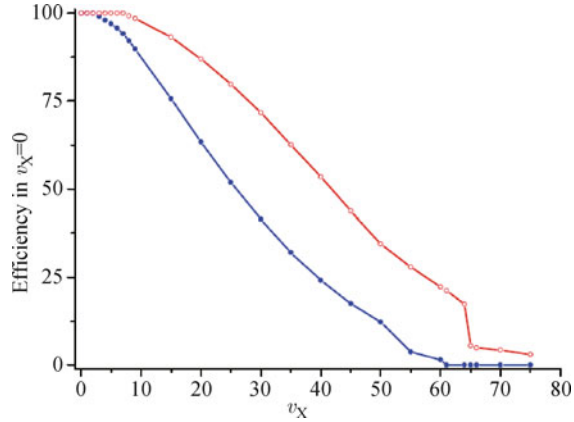

Fig. 8 Numerical simulation evaluating the transfer efficiency of molecules initially in a given v_X toward the ground vibrational $v_X = 0$ for a two broadband lasers with bandwidth similar to one used in the experiment (200 cm^{-1}, *blue line*) and a laser twice broaden (400 cm^{-1}, *red line*).

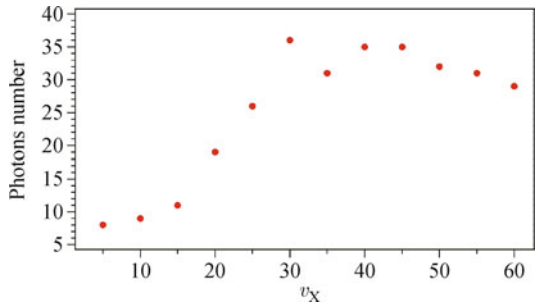

Fig. 9 Total number of photons necessary to transfer cesium molecules from a given vibrational level $v_X \leqslant 10$ toward $v_X = 0$.

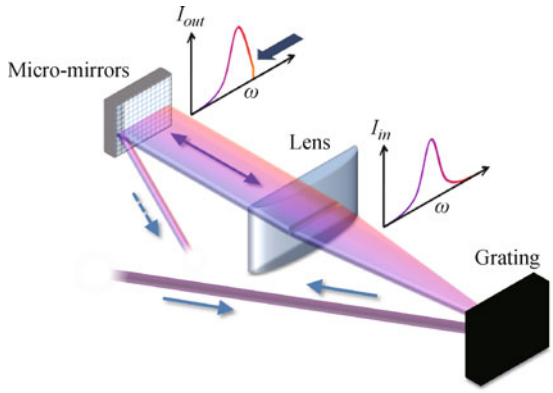

Fig. 10 Schematic representation of the 4-f line used for the shaping of the broadband laser (from right to left: diffraction grating, cylindrical lens $f = 100$ mm, micro-mirrors) spatially spread the laser spectrum. I_{in} and I_{out} respectively sketch the incident laser beam and the reflected shaped laser beam.

limited laser bandwidth. Additionally, these simulations can be widely used for the preparation of various experiments, because they allow the optimization of several important experimental parameters.

Figure 9 shows the time evolution of the population at different vibrational levels. For a power of the femtosecond laser close to the experimental value (100 mW), we evaluate the number of photons (laser and spontaneous emission) necessary for vibrational cooling from a given v_X toward $v_X = 0$. Roughly 10 photons (5 laser cycles) are required to achieve vibrational cooling from vibrational level $v \leqslant 10$. The transfer of population in the $v_X = 0$ level is nearly saturated after 10 000 pulses, which requires 100 μs.

3.3 Laser system

When performing vibrational cooling via optical pumping, the coherence of the light does not play any role, which means that any collimated and broadband source focused on the molecular sample can be used. The laser spectrum must therefore be shaped. One of the simplest and cheapest solutions is to use a broadband laser diode [40].

The spectral resolution required for spectral shaping is on the order of the vibrational frequency divided by the number of levels involved; however, this is not an issue because, even when considering heavy atoms, vibrational frequencies are higher than hundreds of GHz. The simplest shaping is a basic cut-off of part of the light spectrum using black paper or a simple interference filter [36]. For shaping we use a 4-f imaging system similar to that shown in Fig. 10. The broadband laser is sent to a diffraction grating (1800 lines/mm) that spatially splits the different frequency components and then collimates the beam using a 100-mm cylindrical lens. The resulting beam is selectively reflected backward by a mirror placed in the Fourier plane of the optical system. Because the laser spectrum is spatially spread over the entire mirror, a spatial mask or any means preventing the reflection locally leads to the removal of frequency components. Note that if $v_X = 0$ is the dark state, shaping can be achieved using a simple cut-off above 13 030 cm^{-1} in the laser spectrum. The important aspect here is how well the shaping removes the unwanted transition frequencies. For example, the standard liquid crystal spatial light modulator (SLM), as used here, has an extinction ratio between desired and undesired transition frequencies of 97%, which may result in an imperfect dark state. Therefore, it is preferable to use a spatial mask such as rotatable micro-mirrors [41], used later in our experiment, which have an on-off ratio of 100%.

3.4 Potential energy curves

The basic geometrical characteristics of the potentials involved in the transition affect the form of the corresponding FC parabola, and thus, the efficiency of the optical pumping technique. Here, we outline the criteria that define the applicability of this technique to a given electronic transition. In light of this study, we can consider realistic choices for molecular electronic potentials.

- It is important to consider an electronic transition with good properties in terms of lifetime, coupling strength, laser accessibility, and losses (photo-dissociation, pre-dissociation, photo-ionization, etc.).
- The electronic transition should be as 'closed' as possible, with the assumption that spontaneous emission should return the molecular population after excitation for the initial electronic potential at the largest possible percentage. The molecular population can be lost during the optical pumping process for a variety of reasons such as ionization,

pre-dissociation, and coupling to other electronic potentials.

- The internuclear position of the minimum (equilibrium point) of the excited potential must be as close as possible to the minimum of the ground potential $r_{eA} \approx r_{eX}$. If the objective of optical pumping is to transfer the molecular population to the lowest vibrational state possible, then all frequencies that lie lower than the point A in Fig. 11 should be cut, because if they participate in the process, they lead to an increase in vibration.
- The angle θ indicates the speed of vibrational cooling. The larger this angle, the "faster" the cooling (fewer transitions are required for a certain decrease in vibration). This effect can easily be seen in the "bending" of the parabola's arms up to the point at which they touch the axis. In this case, we can see that all transitions towards $v = 0$ are favored (v_X for the upper arm and v_A for the lower arm).

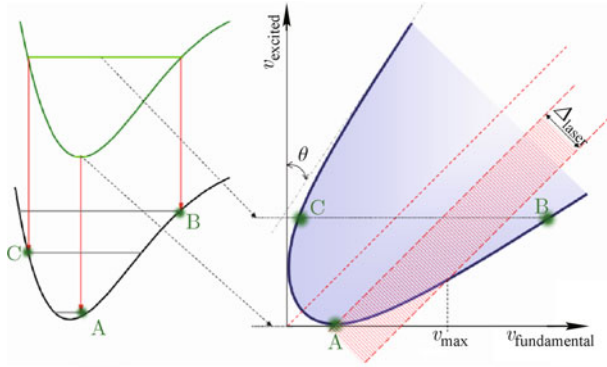

Fig. 11 Schematic representation of the geometric characteristics of the molecular potentials and how they affect the form of the generated Franck–Condon parabola.

3.5 Accumulation in other vibrational levels

The ranging applicability of the optical pumping technique exceeds the case of the ground vibrational level $v_X = 0$. It was demonstrated for other vibrational levels ($v_X = 1$, 2, and 7) using more complex laser shaping [36]. Figure 12 shows the case in which the vibrational level $v_X = 1$ is the target level. Figure 12(a) shows the transitions that can be excited by the pulse-shaped laser (hatched red), which are useful in the study of laser excitation and FC factors for the transitions between

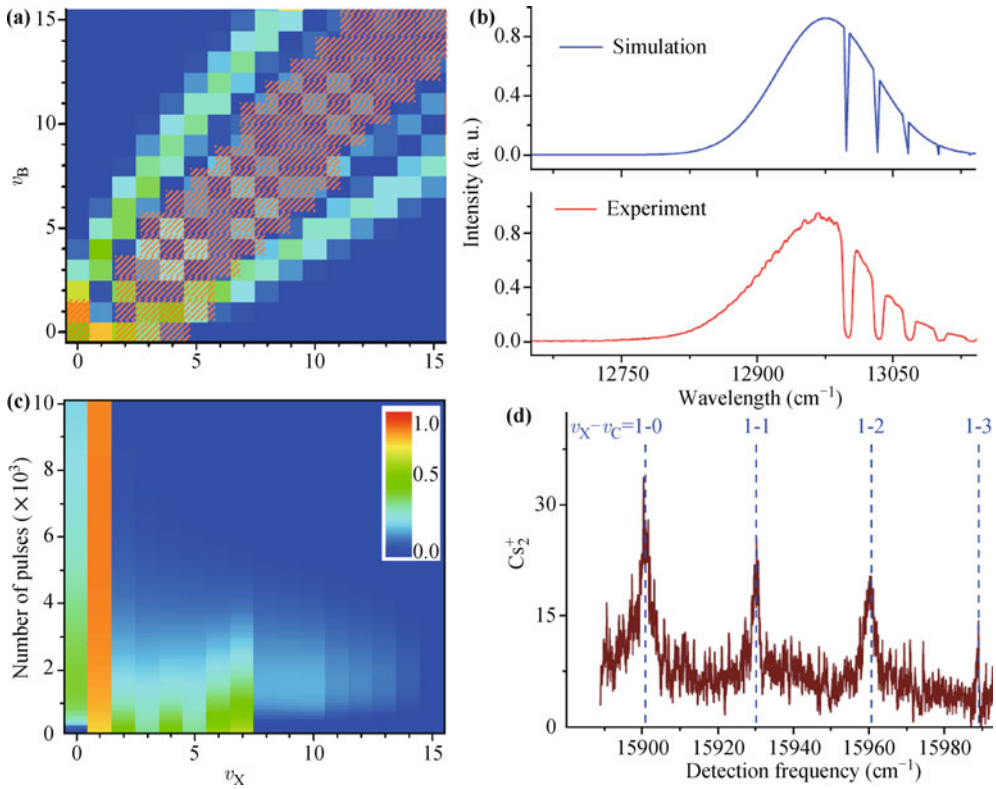

Fig. 12 Simulation and experimental results obtained in the case of $v_X = 1$. **(a)** Franck–Condon parabola for transition between the ground state and the excited state. The hatched (red) area shows the transitions excited by the shaped pulse. **(b)** The laser spectrum used in the simulation (upper one) and in the experiment (lower one). **(c)** Results of the simulation with a color level (log scale) indicating the molecular population in each vibrational level v_X as a function of the number of pulses. **(d)** The obtained photo-ionization spectrum showing a signature of $v_X = 1$ molecules because only transition from $v_X = 1$ to $v_C = 0$ and $v_C = 1$ are present in this spectrum.

the v_X and the v_B vibrational levels, which are, in turn, useful in the study of the spontaneous emission of excited molecules. The required spectrum and the experimental spectrum are shown in Fig. 12(b). Here, we removed any transition frequencies between $v_X = 1$ and any vibrational level v_B of the B state. The result of the simulation is shown in Fig. 12(c); the result predicts a total transfer of 53% to the $v_X = 1$ level. Finally, Fig. 12(d) shows the photo-ionization spectrum in which we can see that the lines corresponding to $v_X = 1 \rightarrow v_C = 0$, 1, 2, and 3 transitions, appear with strong intensity. In principle, any vibrational level can be chosen as the target state. The only challenge arises from the unavailability of a broadband laser that can excite all of the initial molecular distribution; one possibility is the use of a supercontinuum laser.

3.6 Optimized vibrational cooling

To optimize the efficiency of the vibrational cooling process, i.e., the number of molecules transferred to the target vibrational level, more complex pulse shaping should be used. Here, we used the case of a "comb" of selected laser frequencies chosen in such a way that only the transition required to produce efficient optical pumping from the initially populated vibrational levels to the target vibrational level is used. To obtain this optimized spectrum, many approaches can be followed. One approach is maximizing the FC coefficients between the excited states and the target vibrational level. However, because of the limited laser bandwidth, it is more important to limit the transfer of population to high vibrational levels that are not more strongly affected by the laser. Therefore, we have chosen to favor excitation in levels that correspond to the "lower branch" of the FC parabola. With this choice, once a molecule is excited from a vibrational level v_X in this "lower branch", it will decay either to the same v_X level or to the "upper branch" of the FC parabola, i.e., in lower vibrational levels than its initial value.

An example is given in Fig. 13 where the target state is again the $v_X = 1$ level. We use a spatial light modulator to remove all of the frequencies from the laser spectrum except those that excite the various vibrational levels $v_X \neq 1$ to vibrational levels v_B that decay to levels $v'_X \leqslant v_X$. The required pulse is shown in Fig. 13(b). The simu-

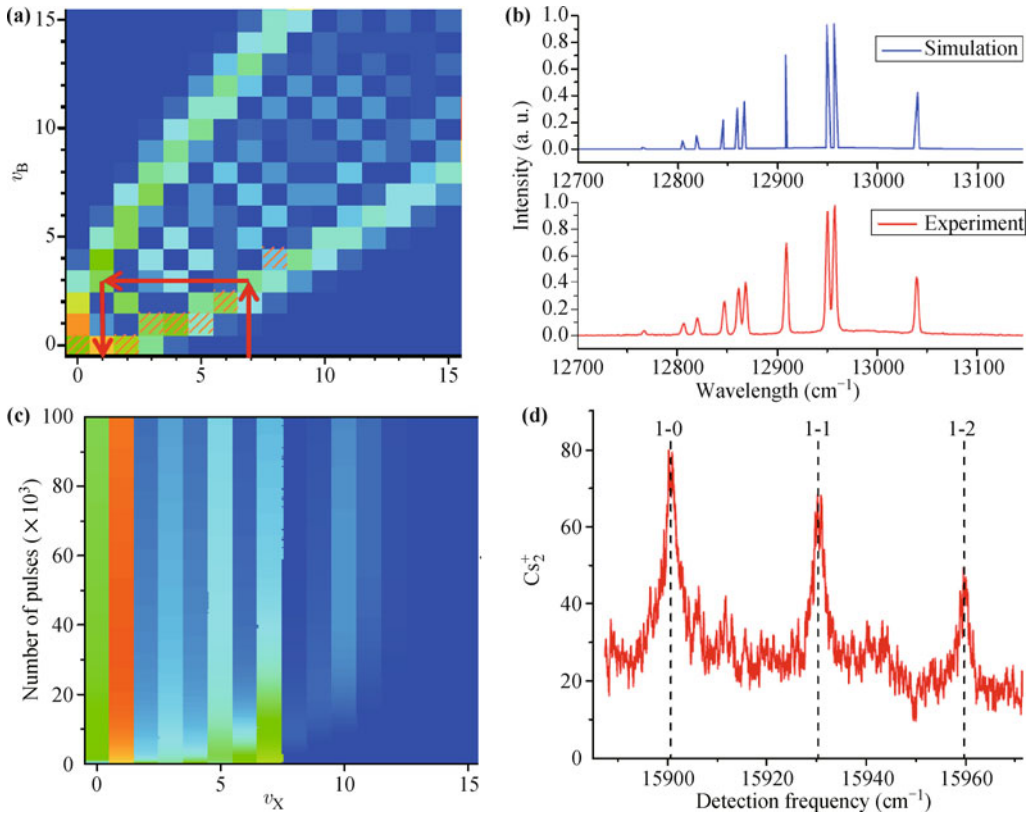

Fig. 13 Population accumulation in $v_X = 1$ by using an optimized shaping. **(a)** FC factors for transition between vibrational levels of X state and B state. The hatched (red) area represents transitions allowed by the shaped laser pulse: i.e., between v_X non-equal to 1 to v_B levels that decay in levels $v'_X \leqslant v_X$. **(b)** The shaped pulse used for the simulation (upper part) and in the experiment (lower part). **(c)** Results of the simulation. **(d)** Experimental detection spectrum showing that mainly $v_X = 1$ molecules are present.

lation is presented in Fig. 13(c); it predicts a transfer of 60%. On the experimental side, in Fig. 13(d), the larger signal, relative to the corresponding signal in Fig. 12(d), indicates that the transfer of population, in the "comb" pulse case, is indeed more efficient than using the "hole" pulse case.

In conclusion, we note that after the first realization of vibrational cooling of Cs_2 molecules, some preliminary results have also been obtained for Rb_2 molecules. These results demonstrate continuous production of vibrationally cooled Rb_2 molecules in three steps [42]. First, they use a dedicated photo-association laser to produce molecules at high vibrational levels of the $X^1\Sigma_g^+$ state. Second, a broadband fiber laser at 1 071 nm is used to transfer the molecules to lower vibrational levels via optical pumping via the $A^1\Sigma_u^+$ state. This process transfers the molecules from vibrational levels around $v'' = 113$ to a distribution of levels where $v'' \leqslant 35$. Then, molecules may be further cooled using a broadband super-luminescent diode at roughly 685 nm with a shaped frequency spectrum. The resulting vibrational distributions are probed using resonance-enhanced multi-photon ionization with a pulsed dye laser at roughly 670 nm.

3.7 Vibrational cooling of heteronuclear molecules: NaCs case

Recently, the vibrational cooling has been successfully demonstrated for polar NaCs molecules [34]. The lack of gerade-ungerade symmetry in hetero-nuclear molecules enables other electronic transitions and different schemes are possible. The initial vibrational distribution of molecules in the ground electronic state $X^1\Sigma^+$ is $v \approx$ 4–6. The optical pumping approach was based on the use of simple, commercially available multimode diode lasers selected to optically pump the population into v_X=0. The ground state molecules are pumped using a 300 mW CW laser covering the 979–991 nm region. This laser is able to excite low vibrational levels toward the $A^1\Sigma^+$-$b^3\Pi$ complex. Because of spin-orbit coupling, the excited molecules can also decay toward the $a^3\Sigma^+$ states, where the same laser can re-excite them. To increase the efficiency, high vibrational levels are excited using a second laser (1.5 W, 6 nm linewidth, 1203–1209 nm). Both lasers have 1-mm waists and were not shaped. The authors also investigated the impact of the cooling process on the rotational state distribution of the vibrational ground state. For rotation, they obtained an initial distribution of $J = 0$–2, which becomes moderately spread after the vibrational cooling process ($J = 0$–4).

We performed a simulation using the excited electronic state $(2)^1\Pi$, which can lead to efficient vibrational cooling of NaCs molecules. In this section, we show the results of a simulation of vibrational cooling of NaCs with the excited electronic state $(2)^1\Pi$. The pulses have Gaussian shape; we start with an equidistribution of the 11 first vibrational levels. Note that no spontaneous emission towards a potential other than the ground state is taken into consideration. In the left column of Fig. 14, we show vibrational cooling with a simply shaped pulse, where all of the frequencies that can excite the population from the $v_X = 0$ level have been removed. As we see in Fig. 14(c) of this column, this pulse can transfer ≈50% of the total molecular population to the ground vibrational level. If an optimized pulse is considered (middle column), a higher percentage of ≈66% can be transferred to the level $v_X = 3$. This level is now the level with the highest FC coefficient; the pulse considered here follows the natural tendencies of the FC-dipole parabola. A percentage of ≈10% is left in the $v_X = 0$ state because of the small value of the FC coefficient corresponding to the $v_X = 0 \rightarrow v_B = 0$ transition, which does not permit efficient pumping of the molecular population out of this state. However, the level $v_X = 0$ can be coupled to other vibrational states because other FC coefficients, such as those connecting to $v_B = 3$ or 4, have high values. This situation permits us to perform the following trick, as shown in the right column of Fig. 14. The transition $v_X = 3 \rightarrow v_B = 0$ is now addressed, whereas $v_X = 0 \rightarrow v_B = 2$ is not, and thus, $v_X = 0$ is now a dark state. This pulse is optimized to transfer the molecular population to the $v_X = 3$ vibrational level; however, the frequency component addressing the $v_X = 3 \rightarrow v_B = 0$ transition manages to 'steal' the molecular population from this level and to bring it to the $v_X = 0$ dark state, where it is accumulated. This pulse results in a transfer of ≈95% of the total molecular population to the ground vibrational level.

4 Rotational cooling

4.1 Detection of rotation

After the photo-association process [$(v,\ J = 8)$ of the 1_g state at 11730.1245 cm^{-1}], only a small number of molecules is produced in any given vibrational level v_X. Consequently, to observe the rotational population, it is useful to increase the number of molecules in each rotational level of $v_X = 0$ by applying the vibrational cooling process. Once molecules are transferred to the ground vibrational level, they are spread over several rotational levels (typically $4 \leqslant J_X \leqslant 14$). This situation can be

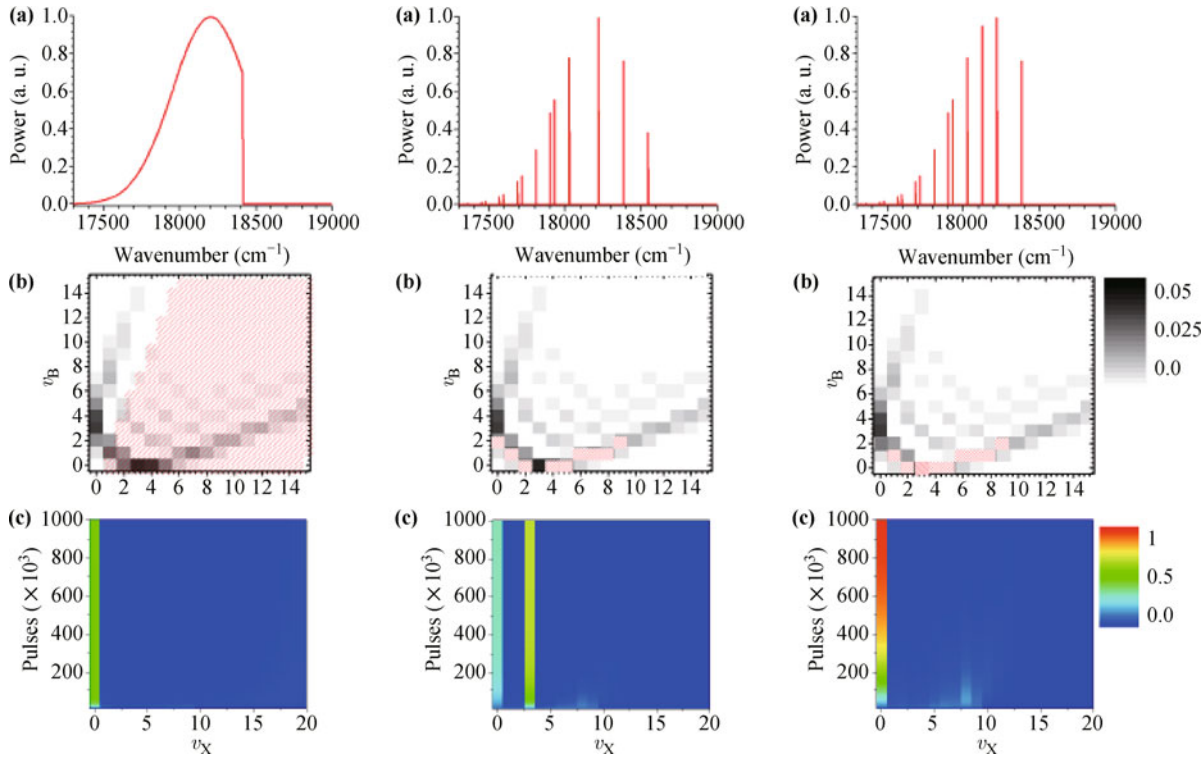

Fig. 14 Left: **(a)** A simply shaped pulse is used in this simulation. All the frequency components that can excite the $v_X = 0$ level are removed. **(b)** The FC-dipole parabola in a linear gray-scale while the red squares correspond to transitions addressed by the pulse shown in (a). **(c)** Simulation with the initial molecular population equally distributed in states with $v_X = 0$–9. After the vibrational cooling, the molecular population in the $v_X = 0$ level has risen from 10% to 51%. Middle: **(a)** An optimized pulse to transfer the molecular population in the $v_X = 3$ level. **(b)** The FC-dipole parabola in a linear gray-scale while the red squares correspond to transitions addressed by the pulse shown in (a). **(c)** Simulation with the initial molecular population equally distributed in states with $v_X = 0$–9. The molecular population transferred to the $v_X = 3$ level is now equal to 66% of the total population. Right: **(a)** The optimized pulse used in this simulation is the same as previously, only that now, $v_X = 3$ is not a dark state while $v_X = 0$ is **(b)** The FC-dipole parabola in a logarithmic gray-scale while the red squares correspond to transitions addressed by the pulse shown in (a). **(c)** Simulation with the initial molecular population equally distributed in states with $v_X = 0$–9. The population transfer to $v_X = 0$ is predicted close to 95%.

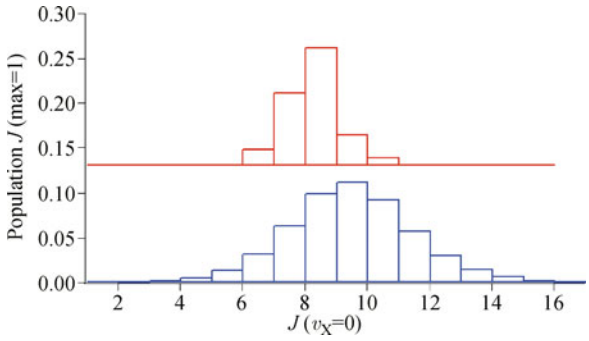

Fig. 15 Rotational distribution of molecules in the ground vibrational level after the photo-association (upper figure) and after the the vibrational cooling (lower figure).

seen in the simulation performed using the Hönl-London factors (Fig. 15).

Another obstacle is that the rotational splitting of Cs_2 levels is too narrow (≈600 MHz); thus, they cannot be resolved using the pulsed dye laser for the vibration, because its line-width is larger than the separation between two rotational levels. For this reason, we have applied other methods that can perform rotational spectroscopy. These methods are based on a continuous narrow-band laser that can selectively excite a rotational level J_X.

4.1.1 Depletion spectroscopy

In depletion spectroscopy [43] we use a continuous-wave (CW) diode laser scanned over a transition $B^1\Pi_u$ (v_B, J_B)← $X^1\Sigma_g^+$ ($v_X = 0$, J_X), which should have a strong FC factor. The narrowband laser quickly pumps the molecular population out of the ground vibrational level; the loss is monitored using the REMPI technique. In Cs_2 molecules case, all of the involved transitions are schematically presented in Fig. 16(a). Briefly, we used a CW DFB laser scanned over the transition $B^1\Pi_u$ ($v_B = 3$, J_B)← $X^1\Sigma_g^+$ ($v_X = 0$, J_X). Even this transition has a small FC factor. We used this transition because of the

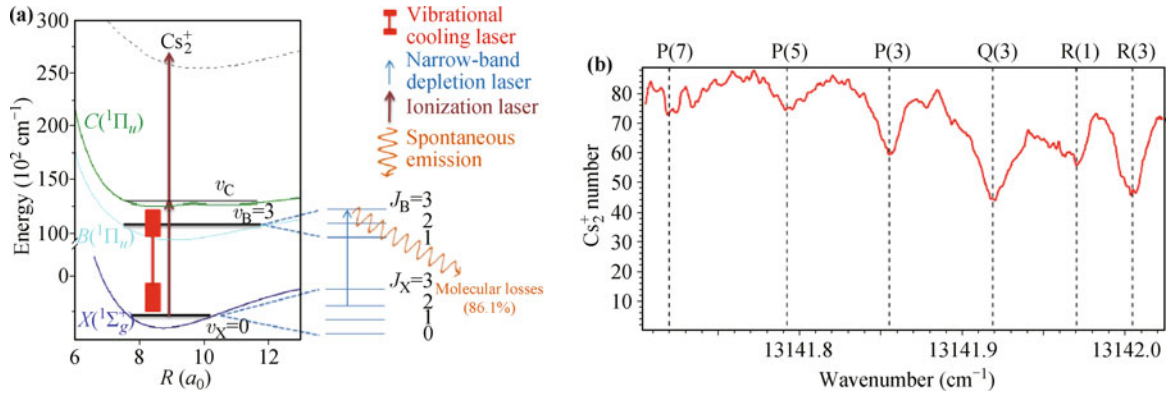

Fig. 16 **(a)** Schematic representation of the transitions involved to resolve the rotational spectrum by the depletion spectroscopy method. **(b)** Depletion spectrum of ground state $v_X = 0$ level. The depletion laser is scanned over ($v_B = 3$, J_B)← ($v_X = 0$, J_X) rotational transitions.

Table 2 Franck–Condon factors (x 100) between $B^1\Pi_u$ (v=3) and $X^1\Sigma_g^+$ (v=0–9) [39].

X	v=0	v=1	v=2	v=3	v=4	v=5	v=6	v=7	v=8	v=9
FC	13.9	17.7	2.8	7.7	10.8	0.4	5.4	**14.4**	14	8.2

limitations on diode lasers at the required wavelength. The population in $v_X = 0$ varies according to the following equations:

$Cs_2(v_X = 0, J_X) + h\nu_{DFB} \rightarrow Cs_2(v_B = 3, J_B = J_X \pm 0, 1)$,

$Cs_2(v_X = 0) + h\nu_{pulsed} \rightarrow Cs_2^*(v_C) + h\nu_{pulsed} \rightarrow Cs_2^+$ (REMPI detection).

When the frequency of the depletion laser is scanned, we acquired a typical depletion spectrum, similar to that shown in Fig. 16(b).

4.1.2 Spontaneous-decay-induced double resonance (SpIDR)

Another detection method of the rotation consists of measuring the spontaneous-decay-induced signal of a vibrational level v_X of the ground electronic state, which has a good FC factor with a vibrational level v_B of the excited electronic state. In Cs_2 case, we chose $v_X = 7$ both because it has the largest FC factor with $v_B = 3$, as shown in Table 2, and because $v_X = 7$ is efficiently emptied by the vibrational optical pumping. Finally, the population in $v_X = 7$ is probed by the pulsed dye laser through the $v_C = 9 \leftarrow v_X = 7$. The various processes involved are summarized below:

$Cs_2(v_X = 0, J_X) + h\nu_{DFB} \rightarrow Cs_2^*(v_B = 3, J_B)$ (excitation),

$Cs_2(v_B = 3, J_B) \rightarrow Cs_2(v_X = 7, J_X) + h\nu_{em}$ (spontaneous emission),

$Cs_2(v_X = 7) + h\nu_{pulsed} \rightarrow Cs_2^*(v_C) + h\nu_{pulsed} \rightarrow Cs_2^*$ (REMPI detection).

The schemes of the laser transitions used to detect rotation using the Spontaneous-decay-induced double resonance (SpIDR) method are shown in Fig. 17(a). The

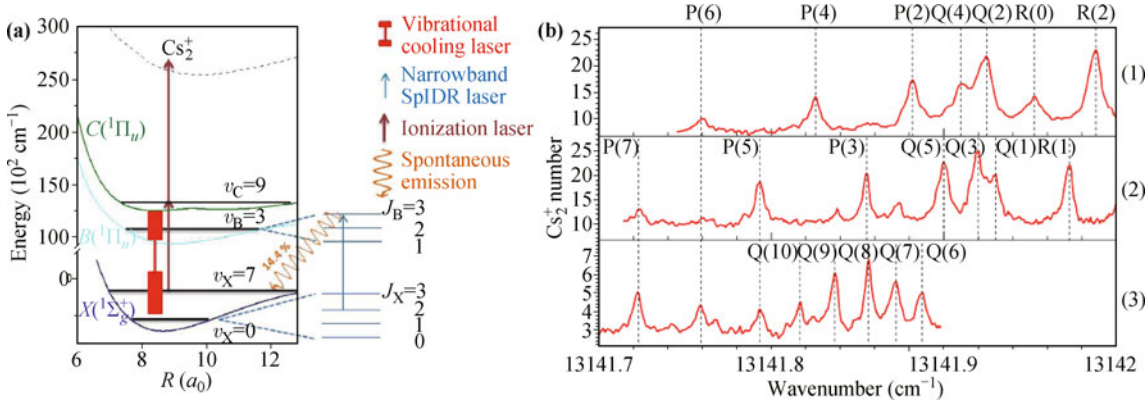

Fig. 17 **(a)** Transitions used to probe the rotational distribution after the optical pumping toward the ground vibrational level. The rotational spectroscopy is performed by a narrow-band SpIDR laser which is scanned over ($v_B = 3$, J_B) ← ($v_X = 0$, J_X) rotational transitions. The brown arrow represents the pulsed laser that ionizes molecules in the $v_X = 7$ level, through the intermediate $C^1\Pi_u$ state ($v_C = 9$). **(b)** Rotational spectra obtained by SpIDR method after vibrational cooling has been applied with three different PA schemes: through (1) 0_g^- ($v = 26$, $J = 1$), (2) 0_g^- ($v = 26$, $J = 2$) and (3) 1_g (v, $J = 8$).

main difference of this method with the depletion method is in the pulsed laser wavelength. As in Ref. [44], we found that this method requires less power and a shorter pulse duration than depletion spectroscopy, despite both methods only differing in their post-ionization step. This situation is caused by the spontaneous-decay-induced signal being almost background-free whereas the depletion signal starts from the fluctuating signal of the $v_X = 0$ population, which strongly alters the signal-to-noise ratio. The spectra obtained via the spontaneous-decay-induced signal method are shown in Fig. 17(b).

Note that we can also use direct ionization of the v_B population after a very fast narrow-band laser pulse according to:

$Cs_2(v_X = 0, J_X) + h\nu_{diode} \rightarrow Cs_2^*(v_B, J_B)$ (selective excitation),

$Cs_2(v_B, J_B) + h\nu_{pulsed} \rightarrow Cs_2^+$ (ionization).

However, it is very difficult to generate such a short pulse using the required narrow-band laser; therefore, we have used other detection methods, as described above.

4.2 Rotational cooling with a broadband laser

To realize rotational cooling, we consider optical pumping with broadband radiation, similar to the method for vibrational cooling. Rotational cooling involves simultaneous excitation of all ro-vibrational levels of the ground electronic state. Shaping of the femtosecond pulse can be used to remove frequencies that excite the absolute ground state of the system $v_X = J_X = 0$, and thus, turn it to a dark state. A similar method of approaching the problem is related to the P, Q, and R transitions, for which the rotation is modified by 0, +1, and –1 respectively. Rotational cooling of the molecular sample can be performed by removing the frequencies corresponding to the transitions $\Delta J = J_A – J_X = 0, +1$ using a simple "cut" in the laser spectrum or by selecting only the P-branch using a shaper with a very high resolution. With this shaping, absorption-spontaneous emission cycles will lead to a decrease in the average principal rotation quantum number J_X, i.e., to laser cooling of the rotation. Note that the rotational degree of freedom cannot be manipulated independently from the vibrational degree of freedom. In fact, vibrational pumping modifies the rotational distribution, just as rotational pumping modifies the vibrational distribution of molecules. In fact, after a single absorption-spontaneous emission cycle, the rotational quantum number can decrease by two units or remain at the same value with a similar probability, i.e., 1/2. However, as the vibrational level is modified by this operation, vibrational pumping is required, which is likely to modify the rotational quantum number again. Figure 19 gives a quantitative analysis of the way vibrational cooling modifies the rotational quantum number. The accumulation of several cycles is, thus, sufficient to efficiently transfer populations to the absolute ro-vibrational ground state ($v = 0$, $J = 0$). As a consequence, global ro-vibrational cooling can be achieved through an interplay between both processes.

In Fig. 18, a plot of the energies that correspond to vibrational transitions between $v_X = 0$ of the ground electronic state ($X^1\Sigma_g^+$) and $v_{B,C} = 0$ of the $B^1\Pi_u$ or $C^1\Pi_u$ state is shown. In the case of the $B^1\Pi_u$ potential, it is not possible to uniquely suppress the transitions starting at $\Delta J = J_B – J_X = 0$ with simple pulse shaping. The situation is different if we consider the state $C^1\Pi_u$. We

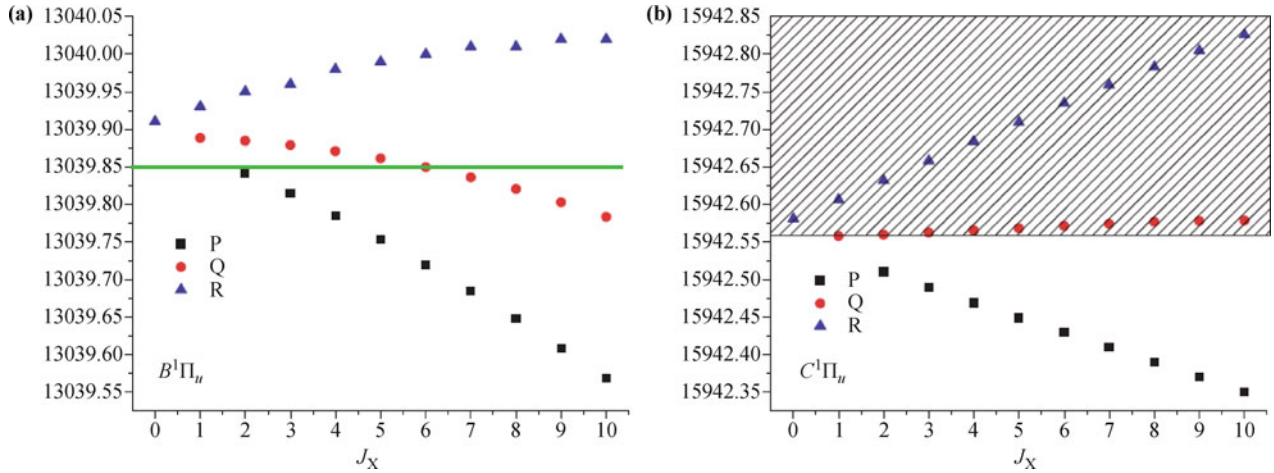

Fig. 18 Ro-vibrationnel transitions energy (Q, R and P branches which correspond to $\Delta J = 0$, 1 and –1, respectively) with the B state **(a)** and with the C state **(b)**. The C state allows a rotational cooling with a simple laser shaping by removing all frequencies larger than 15942.557 cm^{-1}. Such that we ensure that $\Delta J = J_B - J_X = -1$ in each excitation step except for the $J_X = 1$ to $J_C = 1$ transition and the $J_X = 0$ level is now a dark state of the system. However, in the case of B state it is not possible to remove the frequencies with a simple shaping.

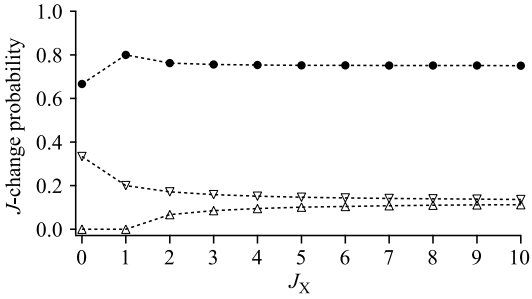

Fig. 19 Effect of vibrational cooling on the rotational distribution: simple Hönl–London formula give the probability to find J_X–2 (*down triangles*), J_X (*circles*), J_X+2 (*up triangles*) from a given J_X after a cycle of absorption/spontaneous emission produced by vibrational cooling.

see that the transitions $\Delta J = J_B - J_X = 0$ can now be suppressed.

One disadvantage related to the choice of the $C^1\Pi_u$ potential instead of the $B^1\Pi_u$ potential is that vibrational cooling cannot be performed via this state. This limitation exists because this state is "shallow" and supports only a small number of vibrational levels (up to $v = 12$). However, the application of two separate cooling pulses (one for vibration and one for rotation, each addressing a different electronic transition), can be considered. Figure 20 shows the results of simulation where the molecules are first vibrationally cooled via the excitation of the state $B^1\Pi_u$ and then rotationally cooled via the excitation of the state $C^1\Pi_u$. The simulation supposes equal power for the two lasers and that each vibrational level has 10 rotational levels. The overall optical pumping process requires 60 000 pulses to transfer a population of 65% of the initial population to the absolute ground state of the system.

Experimentally, in the case of heavy molecules such as Cs_2 molecules, the rotational spectrum is too narrow to be resolved and the shaping considered in the simulation is very difficult to achieve. In fact, the resolution required to excite only the P branch is on the order of ∼600 MHz. If we consider the realization of the required shaping with a 4-f line like that considered for vibrational cooling, the required width of the optical grating is more than one meter. Another complication derives from the fact that we want to perform vibrational and rotational cooling in temporary separated steps. This constraint could become important if the time available to perform our manipulations of the molecules before they exit the MOT volume is limited.

4.3 Rotational cooling with narrow-band laser

As already described, the manipulation of the rotational populations is based on the same principle as that used to achieve the vibrational cooling scheme [45]: a broadband laser excites all of the rotational states except the state of interest, where the molecules accumulate after spontaneous emission. However, in the case of a heavy molecule such as Cs_2, the rotational spectrum is too narrow to be resolved using a simple grating, and thus, the resolution limitation must be improved. To do so, two distinct laser sources are simultaneously used. The first source, devoted to vibrational cooling, is a broadband laser with a spectrum shaped by both a grating and a selective element in the Fourier plane. The second source is a narrow-bandwidth DFB diode laser with a spectrum that is artificially broadened by modulating the diode current so as to obtain a uniform ∼5 GHz scan range. The amplitude, center, speed, and repetition of the scan are controlled by a function generator driving the laser diode current. The effect of temporal scanning is identical to that of a broadband source with the same width. The narrow-band CW diode laser, (∼ 2 MHz, ∼ 6 mW power, 3.5 mm^2 beam size), is continuously scanned

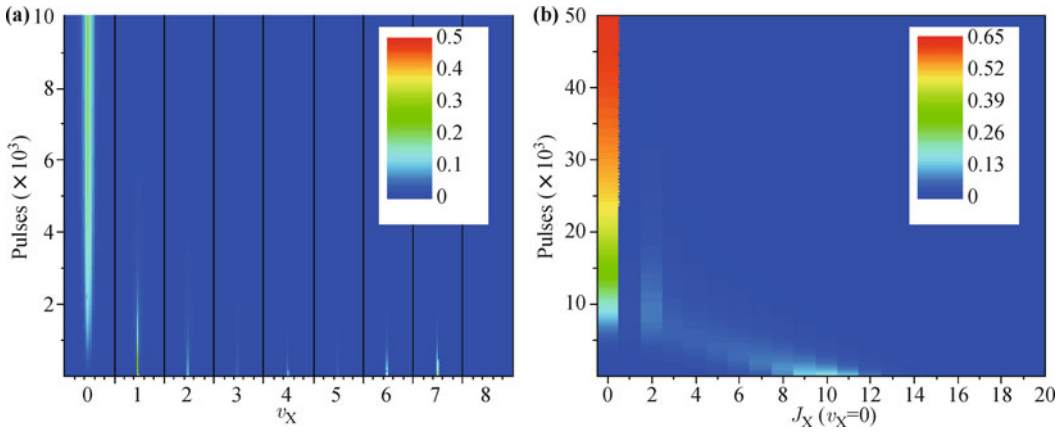

Fig. 20 **(a)** Vibrational cooling via the B state. The plotting is now versus the rotational states, while the vibrational levels are also noted, and the effect of the vibrational cooling in the rotational distribution is shown. **(b)** Rotational cooling via C state. The initial distribution of the part (b) is the final distribution of the vibrational cooling process shown in part (a).

across the correct $B^1\Pi_u(v_B = 3, J_B) \leftarrow X^1\Sigma_g^+(v_X = 0, J_X)$ transitions with a period of 100 μs. As the rotational cooling laser tends to redistribute the molecules in other vibrational levels because of unfavorable FC factors [46], global ro-vibrational cooling is achieved. By studying the FC factors, we learn that the spontaneous decay from $v_B = 3$ populates $v_X \leqslant 10$ primarily, thus providing a global quasi-closed pumping system. Figure 21 shows a typical temporal sequence, allowing for PA and ro-vibrational cooling.

In the experiment to favor a decrease of the J quantum number, the rotational laser spectrum induces only $J_B = J_X - 1$ transitions (P branch). The rotational laser cooling is scanned over the $B^1\Pi_u, v_B = 3, J-1 \leftarrow X^1\Sigma_g^+$, $v_X = 0, J = 2 - 6$. The energies of transitions between rotational levels of $v_X = 0$ and $v_B = 3$ are summarized in Table 3.

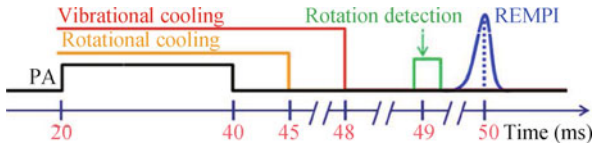

Fig. 21 Temporal sequence used to achieve a global ro-vibrational cooling: PA is applied for 20ms, the rotational and vibrational cooling lasers are applied simultaneously but they are turned off respectively 5ms and 8ms after the PA laser. The rotational detection laser is turned on 1 ms later during typically 50μs. Finally, a pulsed Nd:YAG laser is turned on 1 ms later to detect $X^1\Sigma_g^+$ vibrational levels via the $C^1\Pi_u$ or $D^1\Sigma_u^+$ states.

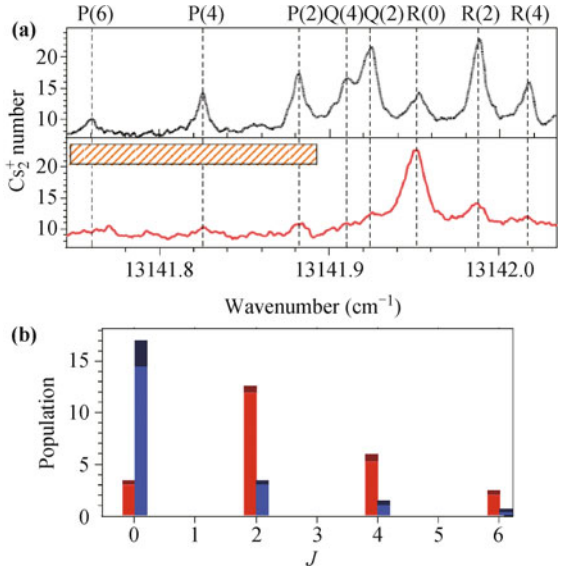

Fig. 22 **(a)** Upper panel: rotational spectrum, obtained by SpIDR, before rotational cooling is applied; Lower panel: rotational spectrum after rotational cooling is applied. The horizontal filled bar represents the frequency range scanned by the DFB rotational pumping laser. **(b)** Population measured in different rotational levels, before (*red bars*) and after (*blue bars*) the cooling phase. The darker colours on the top of the bars indicate the error on the ion numbers.

Table 3 Rotational transition energies between $B^1\Pi_u$ (v=3) and $X^1\Sigma_g^+$ (v=0).

$J_B \leftarrow J_X$	1←2	2←3	3←4	4←5	5←6
E (cm^{-1})	13141.877	13141.85	13141.82	13141.788	13141.755

The resulting spectrum is shown in Fig. 22(a). Figure 22(b) shows the rotational distribution of four levels after vibrational pumping without rotational cooling and when the two cooling lasers are applied. The real number of molecules in a specific rotational state is found by evaluating the FC factor between $v_B = 3$ and $v_X = 7$, and the efficiency of the microchannel plates. Similarly, the Hönl–London factors for P, R, and Q branches are $\frac{1}{4}$, $\frac{1}{4}$, and $\frac{1}{2}$ respectively. Additionally, one absorption-emission cycle decreases the value of J with a probability $p = \frac{3}{4}$ when driving only the P branch. If all of the transitions involved in ro-vibrational cooling permit a decrease in the J value without the creation of a dark state in J for the vibrational cooling step, the J population performs a random walk. After n spontaneous emissions, this random motion will modify the rotational quantum number by $\sqrt{np}$. However, it is possible that the vibrational cooling transitions are not "rotationally" shaped, that is, the vibrational cooling laser, even if shaped for vibrational cooling, still covers all rotational transitions. In this case, the vibrational cooling will counteract the control of the rotation and will create an extra random walk in the process, thereby increasing the rotational quantum number by a probability of $\frac{5}{16}$ at each step. To avoid this undesirable heating, only a small number of vibrational cooling processes can occur between rotational cooling processes. In this case, the efficiency depends on the number of steps required to cool the vibration.

We estimate that the vibrational cooling takes roughly 100 μs to return molecules to $v = 0$ from any vibrational levels. In principle, below 100 μs, a single ramp does not allow complete rotational pumping; however, several cycles give a pumping efficiency equivalent to that obtained with a 100 μs scan period. To estimate the vibrational cooling time, we used the effective laser intensity for a resonance $I_{\text{laser}}^{\text{effectif}} = I_{\text{laser}} \frac{\Gamma}{\Gamma_{\text{laser}}}$ where $\Gamma \approx (2\pi)15$ MHz is the linewidth, I_{laser} is the laser intensity, and Γ_{laser} is the laser bandwidth (~ 100 cm^{-1}). The saturation intensity of a typical ro-vibrational transition is $I_{\text{sat}}^{\text{mol}} = \frac{I_{\text{sat}}}{q_{v',v''}\,\text{HL}}$, where $I_{\text{sat}} \sim 2$ mW/cm^2 is the saturation intensity of the two-level system with a lifetime $\tau = 15$ ns, which is the molecular lifetime in the excited state. We have considered typical FC factors of $q_{v',v''} = 0.1$ and the Hönl–London factor of HL $= \frac{1}{4}$, $I_{\text{sat}}^{\text{mol}} \sim 160$ mW/cm^2. $I_{\text{laser}}^{\text{effectif}} = 10^{-4}$ mW/cm^2 $\simeq \frac{I_{\text{sat}}^{\text{mol}}}{1000} = \frac{I_{\text{sat}}}{10^5}$. The minimum scan period ensuring vibrational pumping is $t = 10^5\tau =$ 100 μs.

5 Perspectives for direct laser cooling of molecules

It was thought that direct laser cooling of molecules is not possible because of the lack of closed transitions in which optical pumping can be realized. However, we see that the technique of vibrational cooling using femtosecond pulses has, in its core, a broadband optical pumping scheme for molecules. Thus, the perspectives offered by the current developments in direct laser cooling of molecules should be studied further. However, the population transfer efficiencies achieved are not able to support optical pumping to achieve laser cooling. The efficiency of the method is reduced by experimental weaknesses that can be overcome. The efficiency of the molecular population transfer can be improved if the femtosecond laser bandwidth is increased, because it would then be more difficult for the molecular population to be trapped in high vibrational levels, i.e., those that are out of the range pumped by the femtosecond laser. In Fig. 23 we see a theoretical study of population transfer toward the $v_X = 0$ state using an optimized femtosecond pulse. The pulse width is three times larger than those used in previous studies, and has a perfect extinction ratio. The efficiency of the population transfer is 99.4%. This level of efficiency is sufficient for the realization of a broadband molecular re-pumper laser for laser cooling of molecules.

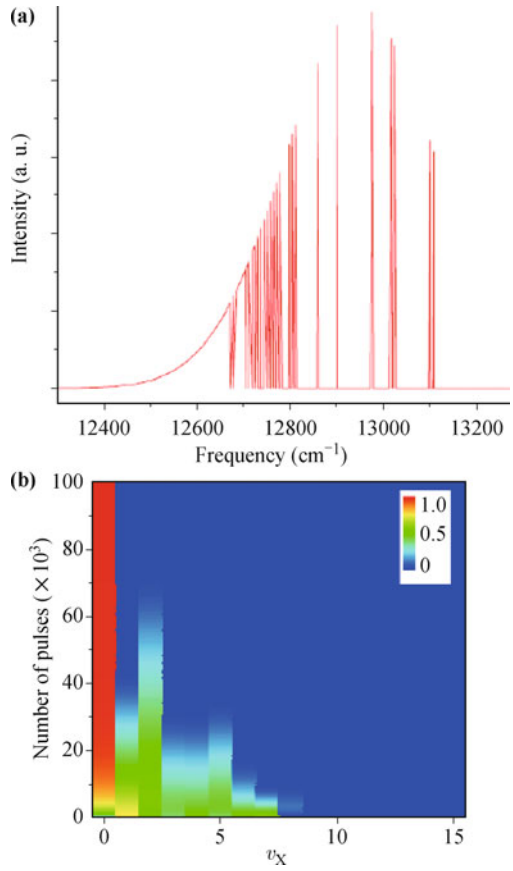

Fig. 23 Simulation for the vibrational cooling by using a shaped pulse three times boarder and with a perfect on-off extinction ratio. **(a)** The shaped pulse used. **(b)** Results of the simulation.

6 Conclusion

We have described the application of an optical pumping technique to efficient transfer of an initial ro-vibrational distribution to a single ro-vibrational level. This method uses light sources to induce efficient absorption-spontaneous emission cycles that lead to a new distribution of the molecular population. Broadband diodes and frequency shaping are cheap, and thus, this scheme can often be easily implemented. This method provides possible schemes for direct laser cooling of molecules [47, 48]. Eventually, photo-association of ultracold cesium molecules in their ground ro-vibrational level with ultracold cesium atoms could lead to the creation of Cs_3 molecules [49] and the study of collisional processes so as to assess the efficiency of evaporative cooling or to investigate methods for achieving controlled chemistry.

References

1. L. D. Carr, D. DeMille, R. V. Krems, and J. Ye, Cold and ultracold molecules: Science, technology and applications, *New J. Phys.* 11(5), 055049 (2009)
2. J. J. Hudson, D. M. Kara,I. J. Smallman, B. E. Sauer, M. R. Tarbutt, and E. A. Hinds, Improved measurement of the shape of the electron, *Nature* 473, 493 (2011)
3. D. S. Jin and J. Ye, Introduction to ultracold molecules: New frontiers in quantum and chemical physics, *Chem. Rev.* 112(9), 4801 (2012)
4. M. Shapiro and P. Brumer, Principles of the Quantum Control of Molecular Processes, Wiley-Interscience, NJ: Hoboken, 2003
5. D. D'Alessandro, Introduction to Quantum Control and Dynamics, Boca Raton: Chapman and Hall, 2007
6. G. Quéméner and P. S. Julienne, Ultracold molecules under control! *Chem. Rev.* 112(9), 4949 (2012)
7. G. Morigi, P. W. H. Pinkse, M. Kowalewski, and R. de Vivie-Riedle, Cavity cooling of internal molecular motion, *Phys. Rev. Lett.* 99(7), 073001 (2007)
8. D. J. Tannor, R. Kosloff, and A. Bartana, Laser cooling of internal degrees of freedom of molecules by dynamically trapped states, *Faraday Discuss.* 113, 365 (1999)
9. S. G. Schirmer, Laser cooling of internal molecular degrees of freedom for vibrationally hot molecules, *Phys. Rev. A* 63(1),

013407 (2000)

10. A. Bartana, R. Kosloff, and D. J. Tannor, Laser cooling of molecular internal degrees of freedom by a series of shaped pulses, *J. Chem. Phys.* 99(1), 196 (1993)
11. C. Brif, R. Chakrabarti, and H. Rabitz, Control of Quantum Phenomena, in: Advances in Chemical Physics, Vol. 148, edited by S. A. Rice and A. R. Dinner, Wiley, 2011
12. E. Shuman, J. Barry, and D. DeMille, Laser cooling of a diatomic molecule, *Nature* 467(7317), 820 (2010)
13. J. F. Barry, E. S. Shuman, E. B. Norrgard, and D. De-Mille, Laser radiation pressure slowing of a molecular beam, *Phys. Rev. Lett.* 108(10), 103002 (2012)
14. M. T. Hummon, M. Yeo, B. K. Stuhl, A. L. Collopy, Y. Xia, and J. Ye, Magneto-optical trapping of diatomic molecules, arXiv: 1209.4069v1
15. M. Zeppenfeld, B. G. U. Englert, R. Glöckner, A. Prehn, M. Mielenz, C. Sommer, L. D. van Buuren, M. Motsch, and G. Rempe, Sisyphus cooling of electrically trapped polyatomic molecules, *Nature* 491(7425), 570 (2012)
16. J. G. Danzl, M. J. Mark, E. Haller, M. Gustavsson, R. Hart, J. Aldegunde, J. M. Hutson, and H.C. Nägerl, An ultracold high-density sample of rovibronic ground-state molecules in an optical lattice, *Nat. Phys.* 6(4), 265 (2010)
17. S. Ospelkaus, K.-K. Ni, G. Quéméner, B. Neyenhuis, D. Wang, M. H. G. de Miranda, J. L. Bohn, J. Ye, and D. S. Jin, Controlling the hyperfine state of rovibronic ground-state polar molecules, *Phys. Rev. Lett.* 104, 030402 (2010), arXiv: 0908.3931
18. G. Pichler, S. Milosevic, D. Viza, and R. Beuc, Diffuse bands in the visible absorption spectra of dense alkali vapours, *J. Phys. At. Mol. Opt. Phys.* 16(24), 4619 (1983)
19. R. B. Jones, J. H. Schloss, and J. G. Eden, Excitation spectra for the photoassociation of Kr–F and Xe–I collision pairs in the ultraviolet (208–258 nm), *J. Chem. Phys.* 98(6), 4317 (1993)
20. U. Marvet and M. Dantus, Femtosecond photoassociation spectroscopy: Coherent bond formation, *Chem. Phys. Lett.* 245(4–5), 393 (1995)
21. T. Ban, S. Ter-Avetisyan, R. Beuc, H. Skenderovic, and G. Pichler, Photoassociation of cesium atoms into the double minimum state, *Chem. Phys. Lett.* 313(1–2), 110 (1999)
22. A. Fioretti, D. Comparat, A. Crubellier, O. Dulieu, F. Masnou-Seeuws, and P. Pillet, Formation of cold Cs_2 molecules through photo association, *Phys. Rev. Lett.* 80(20), 4402 (1998)
23. H. Lignier, A. Fioretti, R. Horchani, C. Drag, N. Bouloufa, M. Allegrini, O. Dulieu, L. Pruvost, P. Pillet, and D. Comparat, Deeply bound cold caesium molecules formed after 0_g^- resonant coupling, *Phys. Chem. Chem. Phys.* 13(42), 18910 (2011)
24. J. Ma, W. Liu, J. Yang, J. Wu, W. Sun, V. S. Ivanov, A. S. Skublov, V. B. Sovkov, X. Dai, and S. Jia, New observation and combined analysis of the $Cs_2 0_g^-$, 0_u^+, and 1_g states at the asymptotes $6S_{1/2} + 6P_{1/2}$ and $6S_{1/2} + 6P_{3/2}$, *J. Chem. Phys.* 141(24), 244310 (2014)
25. A. Fioretti, D. Comparat, C. Drag, C. Amiot, O. Dulieu, F. Masnou-Seeuws, and P. Pillet, Photoassociative spectroscopy of the $Cs_2 0_g^-$ long-range state, *Eur. Phys. J. D* 5(3), 389 (1999)
26. N. Bouloufa, A. Crubellier, and O. Dulieu, Reexamination of the 0_g pure long-range state of Cs_2: Prediction of missing levels in the photoassociation spectrum, *Phys. Rev. A* 75(5), 052501 (2007)
27. K. M. Jones, E. Tiesinga, P. D. Lett, and P. S. Julienne, Ultracold photoassociation spectroscopy: Long-range molecules and atomic scattering, *Rev. Mod. Phys.* 78(2), 483 (2006)
28. R. Horchani, H. Lignier, N. Bouloufa-Maafa, A. Fioretti, P. Pillet, and D. Comparat, Triplet-singlet conversion by broadband optical pumping, *Phys. Rev. A* 85(3), 030502 (2012)
29. M. Raab, G. Höning, W. Demtröder, and C. R. Vidal, High resolution laser spectroscopy of Cs_2 (II): Doppler-free polarization spectroscopy of the $C^1\Pi_u \leftarrow X^1\Sigma_g^+$ system, *J. Chem. Phys.* 76(9), 4370 (1982)
30. W. Weickenmeier, U. Diemer, M. Wahl, M. Raab, W. Demtröder, and W. Müller, Accurate ground state potential of Cs_2 up to the dissociation limit, *J. Chem. Phys.* 82(12), 5354 (1985)
31. R. L. Brooks and J. L. Hunt, Helium hydride emission spectra at 550 and 640 nm, *J. Chem. Phys.* 89(3), 7077 (1988), http://dx.doi.org/10.1063/1.455337
32. A. Wakim, P. Zabawa, M. Haruza, and N. P. Bigelow, Luminorefrigeration: Vibrational cooling of NaCs, *Opt. Express* 20(14), 16083 (2012)
33. T. Schneider, B. Roth, H. Duncker, I. Ernsting, and S. Schiller, All-optical preparation of molecular ions in the rovibrational ground state, *Nat. Phys.* 6(4), 275 (2010)
34. P. F. Staanum, K. Höjbjerre, P. S. Skyt, A. K. Hansen, and M. Drewsen, Rotational laser cooling of vibrationally and translationally cold molecular ions, *Nat. Phys.* 6(4), 271 (2010)
35. M. Viteau, A. Chotia, M. Allegrini, N. Bouloufa, O. Dulieu, D. Comparat, and P. Pillet, Optical pumping and vibrational cooling of molecules, *Science* 321(5886), 232 (2008)
36. D. Sofikitis, S. Weber, A. Fioretti, R. Horchani, M. Allegrini, B. Chatel, D. Comparat, and P. Pillet, Molecular vibrational cooling by optical pumping with shaped femtosecond pulses, *New J. Phys.* 11(5), 055037 (2009)
37. A. Kastler, Quelques suggestions concernant la production optique et la détection optique d'une inégalité de population des niveaux de quantifigation spatiale des atomes. Application à l'expérience de Stern et Gerlach et à la résonance magnétique, *J. Phys. Radium* 11(6), 255 (1950)
38. J. T. Bahns, W. C. Stwalley, and P. L. Gould, Laser cooling of molecules: A sequential scheme for rotation, translation, and vibration, *J. Chem. Phys.* 104(24), 9689 (1996)

39. U. Diemer, R. Duchowicz, M. Ertel, E. Mehdizadeh, W. Demtröder, Doppler-free polarization spectroscopy of the $B^1\Pi_u$ state of Cs_2, *Chem. Phys. Lett.* 164(4), 419 (1989)
40. D. Sofikitis, R. Horchani, Xiaolin Li, M. Pichler, M. Allegrini, A. Fioretti, D.Comparat, and P. Pillet, Vibrational cooling of cesium molecules using noncoherent broadband light, *Phys. Rev. A* 80, 051401(R) (2009)
41. R. Horchani, Femtosecond laser shaping with digital light processing, *Opt. Quantum Electron.* 47(8), 3023 (2015)
42. J. Tallant and L. Marcassa, Continunous vibrational cooling of ground state Rb_2, *Bull. Am. Phys. Soc.* 59, 3004 (2014)
43. D. Wang, C. Ashbaugh, J. T. Kim, E. E. Eyler, P. L. Gould, and W. C. Stwalley, Rotationally resolved depletion spectroscopy of ultracold KRb molecules, *Phys. Rev. A* 75(3), 032511 (2007)
44. K. Aikawa, D. Akamatsu, M. Hayashi, K. Oasa, J. Kobayashi, P. Naidon, T. Kishimoto, M. Ueda, and S. Inouye, Coherent transfer of photoassociated molecules into the rovibrational ground state, *Phys. Rev. Lett.* 105, 203001 (2010), arXiv: 1008.5034
45. I. Manai, R. Horchani, H. Lignier, P. Pillet, D. Comparat, A. Fioretti, and M. Allegrini, Rovibrational cooling of molecules by optical pumping, *Phys. Rev. Lett.* 109, 183001 (2012), and Viewpoint: N. Bigelow, Deep molecular cooling, *Physics* 5, 121 (2012)
46. A. Fioretti, D. Sofikitis, R. Horchani, X. Li, M. Pichler, S. Weber, M. Allegrini, B. Chatel, D. Comparat, and P. Pillet, Cold cesium molecules: From formation to cooling, *J. Mod. Opt.* 56, 2089 (2009)
47. J. T. Bahns, W. C. Stwalley, and P. L. Gould, Laser cooling of molecules: A sequential scheme for rotation, translation, and vibration, *J. Chem. Phys.* 104(24), 9689 (1996)
48. M. D. Rosa, Laser-cooling molecules, *Eur. Phys. J. D* 31(2), 395 (2004)
49. J. Pérez-Ríos, M. Lepers, and O. Dulieu, Theory of long-range ultracold atom-molecule photoassociation, *Phys. Rev. Lett.* 115(7), 073201 (2015)